

**ELECTRICAL AND DIELECTRIC PROPERTIES OF SOLID
AND NANOCOMPOSITE POLYMER ELECTROLYTES
BASED ON CHITOSAN**

SHUJAHADEEN BAKR AZIZ

**THESIS SUBMITTED IN FULFILLMENT OF
THE REQUIREMENT FOR THE DEGREE
OF DOCTOR OF PHILOSOPHY**

**DEPARTMENT OF PHYSICS
FACULTY OF SCIENCE
UNIVERSITY OF MALAYA
KUALA LUMPUR**

2012

UNIVERSITI MALAYA

ORIGINAL LITERARY WORK DECLARATION

Name of Candidate: **Shujahadeen Bakr Aziz** (I.C/Passport No: **G2145414**)

Registration/Matric No: **SHC080051**

Name of Degree: **Doctor of Philosophy, PhD**

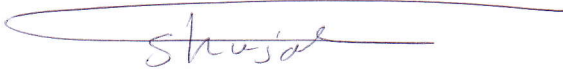
Title of Project Paper/Research Report/Dissertation/Thesis ("this Work"):

**ELECTRICAL AND DIELECTRIC PROPERTIES OF SOLID AND NANOCOMPOSITE
POLYMER ELECTROLYTES BASED ON CHITOSAN**

Field of Study: **Advanced Materials**

I do solemnly and sincerely declare that:

- (1) I am the sole author/writer of this Work;
- (2) This Work is original;
- (3) Any use of any work in which copyright exists was done by way of fair dealing and for permitted purposes and any excerpt or extract from, or reference to or reproduction of any copyright work has been disclosed expressly and sufficiently and the title of the Work and its authorship have been acknowledged in this Work;
- (4) I do not have any actual knowledge nor do I ought reasonably to know that the making of this work constitutes an infringement of any copyright work;
- (5) I hereby assign all and every rights in the copyright to this Work to the University of Malaya ("UM"), who henceforth shall be owner of the copyright in this Work and that any reproduction or use in any form or by any means whatsoever is prohibited without the written consent of UM having been first had and obtained;
- (6) I am fully aware that if in the course of making this Work I have infringed any copyright whether intentionally or otherwise, I may be subject to legal action or any other action as may be determined by UM.



Candidate's Signature

Shujahadeen Bakr Aziz

Date

9 May 2012

Subscribed and solemnly declared before,



Witness's Signature

Date

9 May 2012

Name: **Dr. Zul Hazrin Bin Zainal Abidin**

Designation: Senior lecturer

DR. ZUL HAZRIN ZAINAL ABIDIN
PENSYARAH
JABATAN FIZIK, FAKULTI SAINS
UNIVERSITI MALAYA
50603 KUALA LUMPUR

ABSTRACT

In solid polymer electrolytes (SPEs) and nano-composite polymer electrolytes (NCPEs) the ion conduction mechanism is still not well understood. This motivates us to study the electrical and dielectric properties of solid polymer electrolytes (CS:AgTf, CS:LiTf and CS:NaTf) and nano-composite polymer electrolytes $((1-x)(0.9\text{CS}:0.1\text{AgTf})-x\text{Al}_2\text{O}_3$ ($0.02 \leq x \leq 0.1$), $(1-x)(0.9\text{CS}:0.1\text{NaTf})-x\text{Al}_2\text{O}_3$ ($0.02 \leq x \leq 0.1$) and $(1-x)(0.9\text{CS}:0.1\text{LiTf})-x\text{Al}_2\text{O}_3$ ($0.02 \leq x \leq 0.1$)) based on chitosan. In the present work the SPEs and NCPEs were prepared by the solution cast technique. The XRD results reveal the increase of amorphous fraction in chitosan upon the addition of salts. The UV-vis, TEM, SEM and EDX analysis confirms the formation of metallic silver nanoparticle in CS:AgTf system. The dependence of DC conductivity and dielectric constant on salt concentration is almost the same. In CS:AgTf, CS:NaTf and CS:LiTf systems the DC conductivity follows the Arrhenius equation. The DC conductivity and dielectric constant for these SPEs have been correlated at different temperatures. The pre-exponential factor is independent on dielectric constant and temperature for these SPEs. The broadness of loss tangent peaks and incomplete semicircles of Argand plots reveals the non-Debye relaxation. The impedance plots and AC conductivity spectra at different temperatures were used to confirm the effect of electrode polarization on AC conductivity dispersion. The calculated frequency exponent (s) at different temperatures was used to characterize ion conduction model for each system.

To produce NCPEs the Al_2O_3 nanoparticle (size < 50 nm) were added to SPEs (CSA6, CSB6 and CSC6). The XRD results revealed the increase of amorphous regions (small crystallite size) in NCPEs up to 4 wt.% of Al_2O_3 . At high alumina concentration the

crystallinity of these NCPEs are increased. The SEM analysis shows a well dispersed Al_2O_3 nanoparticle at low concentration and a cluster formation at high alumina concentrations. The EDX analysis reveals that the white clusters are mostly alumina nanoparticles. The DC conductivity and bulk dielectric enhancement of these NCPEs reveal the role played by alumina nanoparticles. The curvature of DC conductivity versus $1000/T$ at higher temperatures were observed for these NCPEs. The drop in DC conductivity at a particular temperature for these three NCPEs can be ascribed to the phase transition of alumina ceramic from ferroelectric to paraelectric. The DC conductivity and dielectric constant study performed at different temperatures are well correlated for these NCPEs. However, the pre-exponential factor and dielectric constant cannot be correlated. The pattern of Arrhenius and compensated Arrhenius are almost the same. The broad loss tangent peaks and electric modulus (Argand plots) reveal the distribution of relaxation times. The electrode polarization effect was clearly observed in the study of impedance plots and AC conductivity spectra at different temperatures. The temperature dependences of frequency exponent were used to specify the ion conduction model for each NCPE system.

ABSTRAK

Didalam elektrolit polimer pepejal (EPP) dan elektrolit polimer nano-komposit (EPNK), mekanisma konduksian ion masih belum difahami sepenuhnya. Ini mendorong kami untuk mengkaji tentang sifat elektrik dan dielektrik elektrolit polimer pepejal (CS:AgTf, CS:LiTf dan CS:NaTf) dan elektrolit polimer nano-komposit ((1-x)(0.9CS:0.1AgTf)-xAl₂O₃ (0.02 ≤ x ≤ 0.1), (1-x)(0.9CS:0.1NaTf)-xAl₂O₃ (0.02 ≤ x ≤ 0.1) dan (1-x)(0.9CS:0.1LiTf)-xAl₂O₃ (0.02 ≤ x ≤ 0.1)) berdasarkan kitosan. Dalam kajian ini, EPP dan EPNK disediakan menggunakan teknik pembekasan larutan. Keputusan XRD menunjukkan bahawa pecahan amorfus meningkat apabila garam ditambahkan. Analisis Uv-vis, TEM, SEM dan EDX mengesahkan adanya pembentukan zarah nano logam perak dalam system CS:AgTf. Kebergantungan konduktiviti AT dan dielektrik malar terhadap kepekatan garam adalah hampir sama. Dalam sistem CS:AgTf, CS:LiTf dan CS:NaTf, konduktiviti AT mematuhi persamaan Arrhenius. Konduktiviti AT dan dielektrik malar bagi semua EPP ini telah di hubungkait pada suhu yang berbeza. Faktor pra-eksponen adalah tidak bergantung dengan dielektrik malar dan suhu bagi semua EPP. Kelebaran puncak tangen kehilangan dan ketidaksempurnaan semibulatan plot Argand membuktikan kelonggaran bukan-Debye. Plot impedans dan konduktiviti AU graf pada suhu yang berbeza telah digunakan untuk membuktikan kesan pengutuban elektrod ke atas penyerakan konduktiviti AU. Eksponen frekuensi yang telah dikira pada suhu yang berbeza telah digunakan untuk mencirikan model kekonduksian ion bagi setiap sistem.

Untuk menghasilkan EPNK, zarah nano Al₂O₃ (saiz < 50 nm) telah dicampurkan ke dalam EPP (CS:AgTf, CS:LiTf dan CS:NaTf). Analisa XRD menunjukkan peningkatan bahagian amorfus (saiz kristal yang kecil) dalam EPNK sehingga 4 wt.%

Al_2O_3 . Pada kepekatan alumina yang tinggi, pengkristalan sampel EPNK meningkat. Analisa SEM menunjukkan taburan Al_2O_3 yang sekata pada kepekatan yang rendah manakala pembentukan kelompok pada kepekatan alumina yang tinggi. Analisa EDX membuktikan bahawa kelompok putih adalah kebanyakannya merupakan zarah nano alumina. Peningkatan konduktiviti AT dan dielektrik EPNK menunjukkan peranan yang dimainkan oleh nano-partikel alumina. Kelengkungan konduktiviti AT melawan $1000/T$ pada suhu tinggi telah diperhatikan bagi EPNK ini. Kejatuhan dalam konduktiviti AT pada suhu tertentu bagi tiga EPNK ini boleh digambarkan sebagai peralihan fasa bagi seramik alumina dari feroelektrik kepada paraelektrik. Kajian konduktiviti AT dan dielektrik malar yang telah dijalankan pada suhu yang berbeza. Walaubagaimanapun, faktor pra-eksponen dan dielektrik malar tidak dapat dikaitkan. Bentuk graf Arrhenius dan imbalan Arrhenius adalah seakan sama. Kelebaran puncak pada tangen kehilangan dan modulus elektrik (plot Argand) menunjukkan taburan masa kelonggaran. Kesan elektrod pengutuban dapat dilihat dengan jelas dalam kajian ini melalui plot impedan graf konduktiviti AU pada suhu berbeza. Kebergantungan suhu terbadap gelombang telah digunakan untuk menyatakan model kekonduksian ion untuk setiap sistem EPNK.

ACKNOWLEDGEMENT

In the name of almighty Allah, most compassionate, most Merciful. I would like to say Alhamdulillah, for giving me the strength, patience and health to complete this work.

I am grateful to express my sincere gratitude and appreciation to my supervisor, Professor Dr. Abdul Kareim Hj Mohd Arof, for his direction, guidance, encouragement and support for completing this thesis. I must mention that without his fatherly help during my study, this thesis could not have been completed. I am also thankful to my co-supervisor, Dr. Zul Hazrin Zainal Abidin for his guidance and support.

I am thankful to Dr. Siti Rohana Majid for her support during my study. I wish to express my appreciation to all of my friends Hamdi, Yap, Kak Mazni, Thompson, Den, Zila, Sim, Teo, Wani, Nabila and Sim for their support and encouragements.

I would like to thank University of Malaya for financial support and Ministry of Higher Education and Scientific Research-Iraq/Kurdistan Regional Government for the scholarship awarded.

I would like to thank my wife, Ahang and my daughter Niga for their support and encouragement. Finally, and most importantly, I would like to express my special gratitude and thanks to my parents for their years of untiring love, support and their prayers. They have given me so much, and to them I will always be indebted.

Shujahadeen B. Aziz

PUBLICATION

List of Published Article in Journals:

- 1. Shujahadeen B. Aziz, Z. H. Z. Abidin, A. K. Arof, Effect of silver nanoparticles on the DC conductivity in chitosan-silver triflate polymer electrolyte, Physica B: Condensed Matter 405 (2010) 4429-4433.**
- 2. Shujahadeen B. Aziz, Z. H. Z. Abidin, A. K. Arof, Influence of silver ion reduction on electrical modulus parameters of solid polymer electrolyte based on chitosan-silver triflate electrolyte membrane, eXPRESS Polymer Letters 4 (2010) 300-310.**

List of Papers presented at Conferences

- 1. Shujahadeen B. Aziz, Z. H. Z. Abidin, A. K. Arof “ AC conductivity analysis of solid polymer electrolyte based on chitosan:AgCF₃SO₃” presented at the National Workshop on Functional Material (NWFM), 20-21 June 2009, University of Malaya, Kuala Lumpur.**
- 2. Shujahadeen B. Aziz, Z. H. Z. Abidin, A. K. Arof “ DC conductivity analysis of solid polymer electrolyte based on chitosan:NaCF₃SO₃”, presented at the 3rd International Conference on Functional Materials and Devices (ICFMD), 14-17 June 2010, Terengganu, Malaysia.**

CONTENTS**CONTENT**

Abstract	ii
Abstrak	iv
Acknowledgement	vi
List of Publications	vii
Contents	viii
List of Figures	xiii
List of Tables	xxiv
CHAPTER 1: INTRODUCTION	1
CHAPTER 2: LITERATURE REVIEW	
2.1 Introduction	7
2.2 Polymer Electrolyte Classifications	8
2.2.1 Polymer-salt complex or dry solid polymer electrolyte (SPE)	8
2.2.2 Plasticized Polymer Electrolyte (PPEs)	8
2.2.3 Gel Polymer Electrolytes (GPEs)	9
2.2.4 Composite polymer electrolytes (CPEs)	10
2.3 Ion Transport Models in Polymer Electrolytes	11
2.3.1 Arrhenius Model for Ion Transport	12
2.3.2 Vogel–Tammann–Fulcher (VTF) Model for Ion Transport	13
2.4 Role of Dielectric Constant on Ion Conduction	15
2.5 Electrochemical Impedance spectroscopy (EIS)	19
2.5.1 Origin of EIS Theory	19

2.5.2	Complex Impedance Spectroscopy	21
2.5.3	Impedance Plots and Equivalent Circuits	23
2.5.4	Impedance-Related Functions	28
2.6	Chitosan and Chitosan Based Polymer Electrolytes	29
2.6.1	Chitosan Structure and Properties	29
2.6.2	Chitosan Based Electrolyte	31
2.7	Summary	33
CHAPTER 3: EXPERIMENTAL TECHNIQUES		
3.1	Introduction	34
3.2	Experimental Details	35
3.2.1	Raw Materials	35
3.2.2	Preparation of Chitosan:XCF ₃ SO ₃ (X=Ag, Na and Li) SPE thin films	35
3.2.3	Preparation of NCPE thin films using Al ₂ O ₃ as a nano size (size < 50 nm) filler	37
3.3	Electrical Measurements	39
3.4	X-ray diffraction (XRD) Analysis	42
3.5	Ultraviolet -visible absorption spectroscopy (UV-Vis)	45
3.6	Scanning Electron Microscopy (SEM) and Energy Dispersive X-ray (EDX)	46
3.7	Transmission Electron Microscopy (TEM)	49
3.8	Summary	51
CHAPTER 4: STRUCTURAL AND MORPHOLOGICAL STUDY		
4.1	Introduction	52
4.2	Structural and morphological analysis of SPEs based on CS:AgTf	53
4.2.1	XRD analysis of SPE based on CS:AgTf	53
4.2.2	UV-vis and TEM analysis of of SPE based on CS:AgTf	59

4.2.3	SEM and EDX analysis of SPE based on CS:AgTf	62
4.3	Structural and morphological analysis of NCPEs based on $(1-x)(0.9\text{CS}:0.1\text{AgTf})\text{-}x\text{Al}_2\text{O}_3$ ($0.02 \leq x \leq 0.1$)	66
4.3.1	XRD analysis of NCPE based on $(1-x)(0.9\text{CS}:0.1\text{AgTf})\text{-}x\text{Al}_2\text{O}_3$ ($0.02 \leq x \leq 0.1$)	66
4.3.2	UV-vis analysis of NCPE based on $(1-x)(0.9\text{CS}:0.1\text{AgTf})\text{-}x\text{Al}_2\text{O}_3$ ($0.02 \leq x \leq 0.1$)	70
4.3.3	SEM and EDX analysis of NCPE based on $(1-x)(0.9\text{CS}:0.1\text{AgTf})\text{-}x\text{Al}_2\text{O}_3$ ($0.02 \leq x \leq 0.1$)	72
4.4	Structural and morphological analysis of SPEs based on CS:NaTf	76
4.4.1	XRD analysis of SPE based on CS:NaTf	76
4.4.2	SEM analysis of SPEs based on CS:NaTf	80
4.5	Structural and morphological analysis of NCPEs based on $(1-x)(0.9\text{CS}:0.1\text{NaTf})\text{-}x\text{Al}_2\text{O}_3$ ($0.02 \leq x \leq 0.1$)	83
4.5.1	XRD analysis of NCPE based on $(1-x)(0.9\text{CS}:0.1\text{NaTf})\text{-}x\text{Al}_2\text{O}_3$ ($0.02 \leq x \leq 0.1$)	83
4.5.2	SEM and EDX analysis of NCPE based on $(1-x)(0.9\text{CS}:0.1\text{NaTf})\text{-}x\text{Al}_2\text{O}_3$ ($0.02 \leq x \leq 0.1$)	86
4.6	Structural and morphological analysis of SPEs based on CS:LiTf	89
4.6.1	XRD analysis of SPEs based on CS:LiTf	89
4.6.2	SEM analysis of SPEs based on CS:LiTf	93
4.7	Structural and morphological analysis of NCPEs based on $(1-x)(0.9\text{CS}:0.1\text{LiTf})\text{-}x\text{Al}_2\text{O}_3$ ($0.02 \leq x \leq 0.1$)	95
4.7.1	XRD analysis of NCPEs based on $(1-x)(0.9\text{CS}:0.1\text{LiTf})\text{-}x\text{Al}_2\text{O}_3$ ($0.02 \leq x \leq 0.1$)	95
4.7.2	SEM and EDX analysis of NCPEs based on $(1-x)(0.9\text{CS}:0.1\text{LiTf})\text{-}x\text{Al}_2\text{O}_3$ ($0.02 \leq x \leq 0.1$)	98
4.8	Summary	102
CHAPTER 5: EIS STUDY ON THE SOLID POLYMER ELECTROLYTES (SPEs)		
5.1	Introduction	104

5.2	Electrical/Dielectric properties of SPEs based on CS:AgTf	105
	5.2.1 DC conductivity and Dielectric analysis of SPE based on CS:AgTf	105
	5.2.2 Frequency dependence of $\tan \delta$ for CS:AgTf (CSA6) SPE	116
	5.2.3 Electric modulus analysis of CSA6 system: Relaxation processes	118
	5.2.4 Correlation between impedance and AC conductivity (σ_{ac}) of SPE based on CS:AgTf (CSA6)	122
5.3	Electrical/Dielectric properties of SPEs based on CS:NaTf	132
	5.3.1 DC conductivity and Dielectric analysis of SPE based on CS:NaTf	132
	5.3.2 Frequency dependence of $\tan \delta$ for CS:NaTf (CSB6) SPE	143
	5.3.3 Electric Modulus analysis of CSB6 system: Relaxation processes	145
	5.3.4 Correlation between impedance and AC conductivity (σ_{ac}) of SPE based on CS:NaTf (CSB6)	150
5.4	Electrical/Dielectric properties of SPEs based on CS:LiTf	157
	5.4.1 DC conductivity and Dielectric analysis of SPE based on CS:LiTf	157
	5.4.2 Frequency dependence of $\tan \delta$ of SPE based on CS:LiTf (CSC6)	167
	5.4.3 Electric Modulus Analysis of CSC6 system: Relaxation processes	168
	5.4.4 Correlation between impedance and AC conductivity (σ_{ac}) of SPE based on CS:LiTf (CSC6)	173
5.5	Summary	180

CHAPTER 6: EIS STUDY ON THE NANO-COMPOSITE SOLID POLYMER ELECTROLYTES (NCPEs)

6.1	Introduction	182
6.2	Electrical/Dielectric properties of NCPEs based on (1-	183

x)(0.9CS:0.1AgTf)-xAl ₂ O ₃ (0.02 ≤ x ≤ 0.1)	
6.2.1 DC conductivity and Dielectric analysis of NCPE based on (1-x)(0.9CS:0.1AgTf)-xAl ₂ O ₃ (0.02 ≤ x ≤ 0.1)	183
6.2.2 Frequency dependence of Tanδ for NCPE (CSNA2) system	191
6.2.3 Electric modulus analysis of CSNA2 system: Relaxation processes	193
6.2.4 Correlation between impedance plots and AC conductivity (σ _{ac}) in NCPEs (CSNA2).	197
6.3 Electrical/Dielectric properties of NCPEs based on (1-x)(0.9CS:0.1NaTf)-xAl ₂ O ₃ (0.02 ≤ x ≤ 0.1)	204
6.3.1 DC conductivity and Dielectric analysis of NCPE based on (1-x)(0.9CS:0.1NaTf)-xAl ₂ O ₃ (0.02 ≤ x ≤ 0.1)	204
6.3.2 Frequency dependence of Tan δ for NCPE (CSNB2) system	213
6.3.3 Electric modulus analysis of CSNB2 system: Relaxation processes	215
6.3.4 Correlation between impedance plots and AC conductivity (σ _{ac}) in NCPEs (CSNB2).	219
6.4 Electrical/Dielectric properties of NCPEs based on (1-x)(0.9CS:0.1LiTf)-xAl ₂ O ₃ (0.02 ≤ x ≤ 0.1)	225
6.4.1 DC conductivity and Dielectric analysis of NCPE based on (1-x)(0.9CS:0.1LiTf)-xAl ₂ O ₃ (0.02 ≤ x ≤ 0.1)	225
6.4.2 Frequency dependence of Tan δ for NCPE (CSNC2) system	235
6.4.3 Electric modulus analysis of CSNC2 system: Relaxation processes	236
6.4.4 Correlation between impedance and AC conductivity (σ _{ac}) in NCPE (CSNC2) system	240
6.5 Summary	247
CHAPTER 7: DISCUSSION	249
CHAPTER 8: CONCLUSION AND FUTURE WORKS	261
References	266

LIST OF FIGURES

Figure	Caption	Page
Figure 2.1	Temperature dependence of ionic conductivity of PVA doped with (a) 0 mole%, (b) 5 mol%, (c) 30 mol%, and (d) 20 mol% of NH_4NO_3 [Hema et al., 2009]	13
Figure 2.2	Temperature dependence plots of the conductivity of polymer electrolytes with various EO/Li ratios [Karan et al., 2008].	14
Figure 2.3	Variation of ϵ' as a function of frequency for PVC/PMMA-based electrolytes. LT6 represent PVC:PMMA: LiCF_3SO_3 (18:42:40) system and DB4 represent PVC:PMMA: LiCF_3SO_3 :DBP (11:25:24:40) system. [Ramesh et al., 2002]	17
Figure 2.4	Figure 2.4 Variation of dielectric constant as a function of frequency for different EC concentrations at room temperature [Sheha, 2009]	18
Figure 2.5	Effect of electric field on ions and dipoles [Nahm, 2006].	20
Figure 2.6	Cole-Cole plots and their equivalent circuits for (a) pure resistor, (b) pure capacitor, (c) capacitor and resistor in series, (d) capacitor and resistor in parallel combination and (e) a leaky system [Huggins, 2002].	26
Figure 2.7	Impedance plot of PVAc-DMF- LiClO_4 complex at 303 K [Baskaran et al,2004].	27
Figure 2.8	Structure of (a) chitin and (b) chitosan [López-Chávez et al., 2005].	31
Figure 3.1	Conductivity and dielectric cell measurement.	40
Figure 3.2	Cole-Cole plot for PVA:chitosan blend [Kadir et al., 2010].	41
Figure 3.3	The incident X-rays and reflected X-rays make an angle of θ symmetric to the normal of crystal plane (He, 2009).	43
Figure 3.4	XRD pattern of PVA: LiCF_3SO_3 polymer electrolytes for (a) 95:05, (b) 85:15 and (c) 75:25(Malathi et al., 2010).	44
Figure 3.5	Optical absorbance in (a) Ag-PVA colloid solution and (b) pure PVA(Gautam and Ram, 2010).	46

Figure 3.6	The interactions of an electron beam and sample atoms generating a variety of signals (Williams and Carter, 2009).	47
Figure 3.7	(a) SEM image and (b) EDX of the film of chitosan:AgNO ₃ (Wei et al., 2009).	49
Figure 3.8	Transmission electron images of silver nanoparticles of chitosan-silver nanocomposite (Vimala et al., 2010).	50
Figure 4.1	XRD pattern of pure AgCF ₃ SO ₃ .	53
Figure 4.2	X-ray diffratogram of (a) CSA1 (pure chitosan), (b) CSA2, (c) CSA3, (d) CSA4, (e) CSA5 and (f) CSA6.	54
Figure 4.3	Gaussian fitting of XRD for (a) CSA1, (b) CSA3 and (c) CSA6 samples.	57
Figure 4.4	X-ray diffraction pattern of chitosan-silver triflate complex (CSA6) at (a) 333 K, (b) 363 K and (c) 393 K.	59
Figure 4.5	UV-vis spectra for (a) pure chitosan and (b) chitosan-AgCF ₃ SO ₃ (CSA6).	60
Figure 4.6	UV-vis spectra of chitosan-AgCF ₃ SO ₃ (CSA6) at different temperatures.	61
Figure 4.7	TEM micrograph of silver nanoparticles for CSA6 at room temperature.	62
Figure 4.8	Scanning electron microscopy (SEM) image for (a) CSA2, (b) CSA3, (c) CSA4, (d) CSA5, (e) CSA6 and (f) EDX for spot in box 1.	65
Figure 4.9	XRD patterns of pure Al ₂ O ₃ nanoparticles.	66
Figure 4.10	X-ray diffratogram of (a) CSA6, (b) CSNA1, (c) CSNA2, (d) CSNA3, (e) CSNA4 and (f) CSNA5.	67
Figure 4.11	Gaussian fitting of XRD for (a) CSNA2 (b) CSNA4 and (c) CSNA5 samples.	69
Figure 4.12	UV-vis spectra of (a) CSNA1, (b) CSNA2, (c) CSNA3, (d) CSNA4 and (e) CSNA5 NCPEs.	72
Figure 4.13	Scanning electron microscopy (SEM) image for (a) CSNA1, (b) CSNA2, (c) CSNA3, (d) CSNA4, (e) CSNA5 and (f) EDX for spot in box 1.	75
Figure 4.14	XRD pattern of pure NaCF ₃ SO ₃ salt.	76

Figure 4.15	X-ray diffratogram of (a) CSB1 (pure chitosan), (b) CSB2, (c) CSB3, (d) CSB4, (e) CSB5 and (f) CSB6.	77
Figure 4.16	Gaussian fitting of XRD for (a) CSB2, (b) CSB5 and (c) CSB6 samples.	79
Figure 4.17	Scanning electron microscopy (SEM) image for (a) CSB2, (b) CSB3, (c) CSB4, (d) CSB5 and (e) CSB6.	82
Figure 4.18	X-ray diffratogram of (a) CSB6, (b) CSNB1, (c) CSNB2, (d) CSNB3, (e) CSNB4 and (f) CSNB5.	83
Figure 4.19	Gaussian fitting of XRD for (a) CSNB2, (b) CSNB3 and (c) CSNB5 samples.	85
Figure 4.20	Scanning electron microscopy (SEM) image for (a) CSNB1, (b) CSNB2, (c) CSNB3, (d) CSNB4, (e) CSNB5 and (f) EDX for spot in box 1.	89
Figure 4.21	X-ray diffraction pattern of pure LiCF_3SO_3 salt.	90
Figure 4.22	X-ray diffratogram of (a) CSC1 (pure chitosan), (b) CSC2, (c) CSC3, (d) CSC4, (e) CSC5 and (f) CSC6.	90
Figure 4.23	Gaussian fitting of XRD for (a) CSC2, (b) CSC5 and (c) CSC6 samples.	92
Figure 4.24	Scanning electron microscopy (SEM) image for (a) CSC2, (b) CSC3, (c) CSC4, (d) CSC5 and (e) CSC6.	95
Figure 4.25	X-ray diffratogram of (a) CSC6, (b) CSNC1, (c) CSNC2, (d) CSNC3, (e) CSNC4 and (f) CSNC5.	96
Figure 4.26	Gaussian fitting of XRD for (a) CSNC2, (b) CSNC3 and (c) CSNC5 samples.	98
Figure 4.27	Scanning electron microscopy (SEM) image for (a) CSNC1, (b) CSNC2, (c) CSNC3, (d) CSNC4, (e) CSNC5 and (f) EDX for spot in box 1.	102
Figure 5.1	The ionic conductivity of chitosan with various AgCF_3SO_3 concentrations.	105
Figure 5.2	Temperature dependence of ionic conductivity of chitosan-silver triflate SPEs.	106
Figure 5.3	Composition dependence of dielectric constant for chitosan-silver triflate SPEs at 308 K.	108

Figure 5.4	Composition dependence of bulk dielectric constant for chitosan-silver triflate SPEs at 303 K.	109
Figure 5.5	Bulk dielectric constant and DC conductivity as a function of AgTf salt concentration.	110
Figure 5.6	Frequency dependence of dielectric constant at different temperatures for CSA6 sample.	111
Figure 5.7	Frequency dependence of bulk dielectric constant at different temperatures for CSA6 sample.	111
Figure 5.8	DC conductivity dependence on dielectric constant at, (1) 303, (2) 313, (3) 323, (4) 333, (5) 343, (6) 353 and (7) 363 K for CSA6 sample.	112
Figure 5.9	Compensated Arrhenius equation plotted against the reciprocal temperature for CSA6 system.	113
Figure 5.10	Temperature and dielectric constant dependent of pre-exponential factor (σ_0) at (1)303, (2) 308, (3) 313, (4) 318, (5) 323, (6) 333, (7) 338 and (8) 343 K for CSA6 system.	114
Figure 5.11	Frequency dependence of dielectric loss at different temperatures for CSA6 sample.	115
Figure 5.12	Frequency dependence of loss tangent ($\tan\delta$) at different temperatures for CSA6 sample.	116
Figure 5.13	Temperature dependence of relaxation frequency for CSA6 sample.	117
Figure 5.14	Frequency dependence of M' at different temperature for chitosan-silver triflate (CSA6).	118
Figure 5.15	Frequency dependence of M'' at different temperature for chitosan-silver triflate (CSA6).	119
Figure 5.16	Argand plots for chitosan-silver triflate at (CSA6) at (a) 303 K, (b) 323 K, (c) 333 K and (d) 343 K.	122
Figure 5.17	Impedance plots of chitosan:AgCF ₃ SO ₃ (CSA6) at (a) 308 K, (b) 318 K, (c) 328 K, (d) 338 K, (e) 348 K, (f) 358 K and (g) 368 K.	126
Figure 5.18	AC conductivity spectra of chitosan:AgCF ₃ SO ₃ (90:10) at (a) 308 K, (b) 318 K, (c) 328 K, (d) 338 K, (e) 348 K, (f) 358 K and (g) 368 K.	130

Figure 5.19	Temperature dependence of the frequency exponent s for CSA6 sample.	132
Figure 5.20	DC conductivity as a function of NaCF_3SO_3 concentration.	133
Figure 5.21	Temperature dependence of ionic conductivity for chitosan:NaTf complexes.	134
Figure 5.22	Compositional dependence of dielectric constant for CS:NaTf complexes.	135
Figure 5.23	Compositional dependence of bulk dielectric constant for CS:NaTf complexes.	136
Figure 5.24	Variation of bulk dielectric constant and DC conductivity with various NaTf concentrations.	137
Figure 5.25	Frequency dependence of dielectric constant (ϵ') for CSB6, at different temperatures.	138
Figure 5.26	Frequency dependence of bulk dielectric constant (ϵ') for CSB6 sample, at different temperatures.	139
Figure 5.27	DC conductivity dependence on dielectric constant at, (1) 303, (2) 313, (3) 323, (4) 333, (5) 343, (6) 353 and (7) 363 K for CSB6 sample.	140
Figure 5.28	Compensated Arrhenius equation plotted against the reciprocal temperature for CSB6 system.	141
Figure 5.29	Temperature and dielectric constant dependent of pre-exponential factor (σ_0) at (1)303, (2) 313, (3) 323, (4) 333, (5) 343, (6) 353 and (7) 363 K for CSB6 system.	142
Figure 5.30	Frequency dependence of dielectric loss at different temperatures for CSB6.	143
Figure 5.31	Frequency dependence of loss tangent ($\tan\delta$) for CS:NaTf (CSB6) sample at different temperatures.	144
Figure 5.32	Temperature dependence of relaxation frequency for CSB6 sample.	145
Figure 5.33	Frequency dependence of M' at different temperatures for CSB6 sample.	146
Figure 5.34	Frequency dependence of M'' at different temperatures for CSB6 sample sample.	147

Figure 5.35	Argand plots for CS:NaTf (CSB6) at (a) 303 K, (b) 323 K, (c) 333 K and (d) 343 K.	149
Figure 5.36	Impedance plots of chitosan:NaCF ₃ SO ₃ (CSB6) at (a) 313 K, (b) 333 K, (c) 353 K, (d) 373 K and (e) 413 K	152
Figure 5.37	AC conductivity spectra of chitosan:NaCF ₃ SO ₃ (CSB6) at (a) 313 K, (b) 333 K, (c) 353 K, (d) 373 K, (e) 393 K and (f) 413 K.	156
Figure 5.38	Temperature dependence of the frequency exponent s for CSB6 sample.	157
Figure 5.39	DC conductivity as a function of LiCF ₃ SO ₃ concentration.	158
Figure 5.40	Temperature dependence of ionic conductivity for CS:LiTf SPEs.	159
Figure 5.41	Compositional dependence of dielectric constant for CS:LiTf SPEs.	160
Figure 5.42	Compositional dependence of bulk dielectric constant for CS:LiTf SPEs.	161
Figure 5.43	Variation of dielectric constant and DC conductivity with various LiTf concentrations.	161
Figure 5.44	Frequency dependence of dielectric constant (ϵ') for CSC6, at different temperatures.	162
Figure 5.45	Frequency dependence of bulk dielectric constant (ϵ') for CSC6, at different temperatures.	163
Figure 5.46	DC conductivity dependence on dielectric constant at, (1) 303, (2) 313, (3) 323, (4) 333, (5) 343, (6) 353 and (7) 363 K for CSC6 sample.	164
Figure 5.47	Compensated Arrhenius equation plotted against the reciprocal temperature for CSC6 system.	165
Figure 5.48	Temperature and dielectric constant dependent of pre-exponential factor (σ_0) at (1)303, (2) 313, (3) 323, (4) 333, (5) 343, (6) 353 and (7) 363 K for CSC6 system.	166
Figure 5.49	Frequency dependence of ϵ'' at different temperatures for CSC6 sample.	166
Figure 5.50	Frequency dependence of $\tan\delta$ at different temperatures for CSC6 sample.	167

Figure 5.51	Temperature dependence of relaxation frequency for CSC6 sample.	168
Figure 5.52	Frequency dependence real part (M') of M^* for chitosan:LiCF ₃ SO ₃ (CSC6) at different temperature.	169
Figure 5.53	Frequency dependence of imaginary part (M'') of M^* for chitosan:LiCF ₃ SO ₃ (CSC6) at different temperature.	170
Figure 5.54	Argand plots for chitosan:LiCF ₃ SO ₃ (CSC6) at (a) 303 K, (b) 323 K, (c) 333 K and (d) 343 K.	173
Figure 5.55	Impedance plot of chitosan:LiCF ₃ SO ₃ (CSC6) at (a) 313 K, (b) 333 K, (c) 353 K, (d) 373 K, (e) 393 K and (f) 413 K.	176
Figure 5.56	AC conductivity spectra of chitosan:LiCF ₃ SO ₃ (CSC6) at (a) 313 K, (b) 333 K, (c) 353 K, (d) 373 K, (e) 393 K and (f) 413 K.	179
Figure 5.57	Temperature dependence of the frequency exponent s for CSC6 sample.	180
Figure 6.1	The ionic conductivity of chitosan:AgTf (CSA6) with various concentration of Al ₂ O ₃ .	183
Figure 6.2	Temperature dependence of ionic conductivity of (1-x)(0.9CS:0.1AgTf)-xAl ₂ O ₃ ($0.02 \leq x \leq 0.1$) nano-composite system.	184
Figure 6.3	Composition dependence of dielectric constant for (1-x)(0.9CS:0.1AgTf)-xAl ₂ O ₃ ($0.02 \leq x \leq 0.1$) NCPEs.	185
Figure 6.4	Composition dependence of bulk dielectric constant for (1-x)(0.9CS:0.1AgTf)-xAl ₂ O ₃ ($0.02 \leq x \leq 0.1$) NCPEs.	186
Figure 6.5	Dependence of Bulk dielectric constant and DC conductivity of chitosan:AgTf (CSA6) on Al ₂ O ₃ concentration.	186
Figure 6.6	Frequency dependence of dielectric constant at different temperatures for CSNA2 sample.	187
Figure 6.7	Frequency dependence of bulk dielectric constant at different temperatures for CSNA2.	188
Figure 6.8	DC conductivity dependence on dielectric constant at, (1) 303, (2) 308, (3) 313, (4) 318, (5) 323, (6) 328 and (7) 333 K for CSNA2 sample.	189

Figure 6.9	Compensated Arrhenius equation plotted against the reciprocal temperature for CSNA2 system.	189
Figure 6.10	Temperature and dielectric constant dependent of pre-exponential factor (σ_0) at (1)303, (2) 308, (3) 313, (4) 318, (5) 323, (6) 328 and (7) 333 K for CSNA2 system.	190
Figure 6.11	Frequency dependence of dielectric loss at different temperatures for CSNA2 system.	191
Figure 6.12	Frequency dependence of loss tangent ($\tan\delta$) at different temperatures for CSNA2 sample.	192
Figure 6.13	Temperature dependence of relaxation frequency for CSNA2 system.	192
Figure 6.14	Frequency dependence of M' at different temperature for CSNA2 sample.	193
Figure 6.15	Frequency dependence of M'' at different temperature for CSNA2 sample.	194
Figure 6.16	Argand plots for NCPE (CSNA2) at (a) 303 K, (b) 323 K, (c) 343 K and (d) 353 K.	197
Figure 6.17	Impedance plots for NCPE (CSNA2) at (a) 303 K, (b) 313 K, (c) 323 K, (d) 333 K, (e) 343 K, and (f) 353 K.	200
Figure 6.18	AC conductivity spectra for NCPE (CSNA2) at (a) 303 K, (b) 313 K, (c) 323 K, (d) 333 K, (e) 343 K, and (f) 353 K.	203
Figure 6.19	Temperature dependence of the frequency exponent s for CSNA2 system.	204
Figure 6.20	The ionic conductivity of chitosan:NaTf (CSB6) with various concentration of Al_2O_3 .	205
Figure 6.21	Temperature dependence of ionic conductivity of $(1-x)(0.9CS:0.1NaTf)-xAl_2O_3$ ($0.02 \leq x \leq 0.1$) NCPEs.	206
Figure 6.22	Composition dependence of dielectric constant for $(1-x)(0.9CS:0.1NaTf)-xAl_2O_3$ ($0.02 \leq x \leq 0.1$) NCPEs.	207
Figure 6.23	Composition dependence of bulk dielectric constant for $(1-x)(0.9CS:0.1NaTf)-xAl_2O_3$ ($0.02 \leq x \leq 0.1$) NCPEs.	208
Figure 6.24	Dependence of bulk dielectric constant and DC conductivity of chitosan:NaTf (CSB6) on Al_2O_3 concentration.	208

Figure 6.25	Frequency dependence of dielectric constant at different temperatures for CSNB2 system.	209
Figure 6.26	Frequency dependence of bulk dielectric constant at different temperatures for CSNB2 system.	210
Figure 6.27	DC conductivity dependence on dielectric constant at, (1) 303, (2) 308, (3) 313, (4) 318, (5) 323, (6) 328 and (7) 333 K for CSNB2 system.	211
Figure 6.28	Compensated Arrhenius equation plotted against the reciprocal temperature for CSNB2 system.	211
Figure 6.29	Temperature and dielectric constant dependent of pre-exponential factor (σ_0) at (1)303, (2) 308, (3) 313, (4) 318, (5) 323, (6) 328 and (7) 333 K for CSNB2 system.	212
Figure 6.30	Frequency dependence of dielectric loss at different temperatures for CSNB2 system.	213
Figure 6.31	Frequency dependence of loss tangent ($\tan\delta$) at different temperatures for CSNB2 system.	214
Figure 6.32	Temperature dependence of relaxation frequency for CSNB2 system.	214
Figure 6.33	Frequency dependence of M' at different temperature for CSNB2 sample.	215
Figure 6.34	Frequency dependence of M'' at different temperature for CSNB2 sample.	216
Figure 6.35	Argand plots for NCPE (CSNB2) at (a) 303 K, (b) 323 K, (c) 343 K and (d) 353 K.	218
Figure 6.36	Impedance plots for NCPE (CSNB2) system at (a) 303 K, (b) 313 K, (c) 323 K, (d) 333 K, (e) 343 K, and (f) 353 K.	222
Figure 6.37	AC conductivity spectra for NCPE (CSNB2) system at (a) 303 K, (b) 313 K, (c) 323 K, (d) 333 K, (e) 343 K, and (f) 353 K.	224
Figure 6.38	Temperature dependence of frequency exponent (s) for CSNB2 system.	225
Figure 6.39	The ionic conductivity of chitosan:LiTf (CSC6) with various concentration of Al_2O_3 .	226
Figure 6.40	Temperature dependence of ionic conductivity of $(1-x)(0.9CS:0.1LiTf)-xAl_2O_3$ ($0.02 \leq x \leq 0.1$) NCPEs.	227

Figure 6.41	Composition dependence of dielectric constant for (1-x)(0.9CS:0.1LiTf)-xAl ₂ O ₃ (0.02 ≤ x ≤ 0.1) NCPEs.	228
Figure 6.42	Composition dependence of bulk dielectric constant for CS:LiTf(90:10):xAl ₂ O ₃ (2 ≤ x ≤ 0.1) NCPEs.	229
Figure 6.43	Dependence of Bulk dielectric constant and DC conductivity of chitosan:LiTf (CSC6) on Al ₂ O ₃ concentration.	229
Figure 6.44	Frequency dependence of dielectric constant at different temperatures for CSNC2 system.	230
Figure 6.45	Frequency dependence of bulk dielectric constant at different temperatures for CSNC2 system.	231
Figure 6.46	DC conductivity dependence on dielectric constant at, (1) 303, (2) 308, (3) 313, (4) 318, (5) 323, (6) 328 and (7) 333 K for CSNC2 system.	232
Figure 6.47	Compensated Arrhenius equation plotted against the reciprocal temperature for CSNC2 system.	233
Figure 6.48	Temperature and dielectric constant dependent of pre-exponential factor (σ ₀) at (1)303, (2) 308, (3) 313, (4) 318, (5) 323, (6) 328 and (7) 333 K for CSNC2 system.	233
Figure 6.49	Frequency dependence of dielectric loss at different temperatures for CSNC2 system.	234
Figure 6.50	Frequency dependence of loss tangent (tanδ) at different temperatures for CSNC2 sample.	235
Figure 6.51	Temperature dependence of relaxation frequency for CSNC2 system.	236
Figure 6.52	Frequency dependence of M' at different temperature for CSNC2 sample.	236
Figure 6.53	Frequency dependence of M'' at different temperature for CSNC2 sample.	237
Figure 6.54	Argand plots for NCPE (CSNC2) at (a) 303 K, (b) 323 K, (c) 343 K and (d) 353 K.	240
Figure 6.55	Impedance plots for NCPE (CSNC2) at (a) 303 K, (b) 313 K, (c) 323 K, (d) 333 K, (e) 343 K, and (f) 353 K.	243
Figure 6.56	AC conductivity spectra for NCPE (CSNC2) at (a) 303 K, (b) 313 K, (c) 323 K, (d) 333 K, (e) 343 K, and (f) 353 K.	246

Figure 6.57 Temperature dependence of frequency exponent (s) for 247 CSNC2 system.

LIST OF TABLES

Table	Caption	Page
Table 2.1	Relations between the four basic impedance functions [Barsoukov and Macdonald, 2005].	29
Table 2.2	Examples of chitosan based solid polymer electrolytes.	32
Table 2.3	Examples of plasticized chitosan based polymer electrolyte.	33
Table 3.1	Composition of chitosan:AgCF ₃ SO ₃ SPE samples.	36
Table 3.2	Composition of chitosan:NaCF ₃ SO ₃ SPE samples.	36
Table 3.3	Composition of chitosan:LiCF ₃ SO ₃ SPE samples.	37
Table 3.4	composition of (1-x)(0.9CS:0.1AgTf)-xAl ₂ O ₃ (0.02 ≤ x ≤ 0.1) NCPEs	38
Table 3.5	composition of (1-x)(0.9CS:0.1NaTf)-xAl ₂ O ₃ (0.02 ≤ x ≤ 0.1) NCPEs	38
Table 3.6	composition of (1-x)(0.9CS:0.1LiTf)-xAl ₂ O ₃ (0.02 ≤ x ≤ 0.1) NCPEs	39
Table 4.1	2θ°, FWHM, crystallite size (L) and degree of crystallinity (χ) for selected CS:AgTf SPE samples.	57
Table 4.2	2θ°, FWHM and crystallite size (L) for CSNA2, CSNA4 and CSNA5 NCPEs.	69
Table 4.3	2θ°, FWHM, crystallite size (L) and degree of crystallinity (χ) for CSB2, CSB5 and CSB6 SPEs.	80
Table 4.4	2θ°, FWHM, crystallite size (L) and degree of crystallinity (χ) for CSNB2, CSNB3 and CSNB5 NCPEs.	85
Table 4.5	2θ°, FWHM, crystallite size (L) and degree of crystallinity (χ) for CSC2, CSC5 and CSC6 SPEs.	92
Table 4.6	2θ°, FWHM, crystallite size (L) and degree of crystallinity (χ) for CSNC2, CSNC3 and CSNC5 NCPEs.	98